Evaluating spatiotemporal variations and exposure risk of ground-level ozone concentrations across China from 2000 to 2020 using satellite-derived high-resolution data

Qingqing He[1,2,*], Jingru Cao[1], Pablo E. Saide[2,3], Tong Ye[1], Weihang Wang[1], Ming Zhang[1,*], and Jiejun Huang[1]

[1]School of Resource and Environmental Engineering, Wuhan University of Technology, Wuhan 430070, China
[2]Department of Atmospheric & Oceanic Sciences, University of California, Los Angeles, Los Angeles, California 90095, United States
[3]Institute of the Environment and Sustainability, University of California, Los Angeles, Los Angeles, California 90095, United States

Correspondence: Qingqing He (qqhe@whut.edu.cn) and Ming Zhang (zhangming_88@whut.edu.cn)

Abstract. Understanding the spatial and temporal characteristics of both long- and short-term exposure to ground-level ozone is crucial for refining environmental management and improving health studies. However, such studies have been constrained by the availability of spatiotemporal high-resolution data. To address this gap, we characterized ground-level ozone variations and exposure risks across multiple spatial (pixel, county, region, and national) and temporal (daily, monthly, seasonal, and annual) scales using daily 1-km ozone data from 2000 to 2020, derived from satellite land surface temperature data via a machine-learning hindcast method. The model provided reliable estimates, validated through rigorous cross-validation and direct comparison with external ground-level ozone measurements. Our long-term estimates revealed seasonal shifts in high-exposure ozone centers: spring in eastern China, summer in the North China Plain (NCP), and autumn in the Pearl River Delta (PRD). A non-monotonous trend was observed, with ozone levels rising from 2001-2007 at a rate of 0.47 μg/m^3/year, declining after 2008 (-0.58 μg/m^3/year), and increasing significantly from 2016-2020 (1.16 μg/m^3/year), accompanied by regional and seasonal fluctuations. Notably, ozone levels increased by 0.63 μg/m^3/year in summer in the NCP during the second phase, and by 6.38 μg/m^3/year in autumn in the PRD during the third phase. Exposure levels over 100 μg/m^3 have shifted from June to May, and levels exceeding 160 μg/m^3 were primarily seen in the NCP, showing an expanding trend. Our day-to-day analysis highlights the influence of meteorological factors on extreme events. These findings emphasize the need for increased public health awareness and stronger mitigation efforts.

1 Introduction

Ground-level ozone is a critical pollutant and greenhouse gas in the atmosphere. A growing body of research has demonstrated that both short-term and long-term exposure to ambient ozone are linked to various adverse health outcomes, including asthma (Nicholas et al., 2020) , respiratory tract infections (Burnett et al., 1994), and even premature deaths (Maji and Namdeo, 2021). Moreover, severe ozone pollution in the ambient environment also impacts agriculture crops and contributes to climate change

(Li et al., 2018; Ramya et al., 2023). Therefore, it is crucial to investigate the long-term variation of ground-level ozone, especially for China, a country undergoing significant atmospheric environmental changes due to its rapid economic growth and evolving air pollution control policies over the last two decades. Additionally, influenced by a mix of meteorological conditions, local emissions, and regional transport mechanisms (Fiore et al., 2003; Jaffe, 2011; Monks et al., 2015), ground-level ozone exhibits considerable heterogeneities in its spatial distribution and temporal trend. Understanding these fine-scale variations can provide more precise information about local ozone variations, for example, helping to identify local ozone spikes (Shi et al., 2023; Chen et al., 2022) and allowing for accurate assessments of human exposure to ozone at the community or even neighborhood level (Alexeeff et al., 2018). However, such intricate tasks cannot be accomplished solely by the ground-level air quality monitoring network. While monitoring networks offer accurate ozone concentration data, their limited observation duration and sparse station distribution inadequately capture intraurban variations, often resulting in underestimates of neighborhood and individual exposure variability (Dias and Tchepel, 2018). Therefore, it is necessary to enhance the understanding in ground-level ozone variation and enable more effective mitigation measures using full-coverage, long-term ozone data with high spatiotemporal resolution.

To date, various methods have been employed to address the limitations of ground-level ozone data for a more comprehensive understanding. Atmospheric chemical transport models (CTMs) have been extensively used to simulate ground-level ozone concentrations (Sharma et al., 2017). However, this method typically provides coarse-resolution simulations (usually $\geq$12km×12km) (Qiao et al., 2019; Sun et al., 2019), due to its high computation cost, and its accuracy needs to be improved due to the large uncertainty in the emission inventory and many assumptions made when running the CTM model (Sharma et al., 2017). Advanced statistical/machine-learning algorithms provide an alternative way to obtain spatiotemporal patterns in ozone. By combining with ground-level ozone observations and satellite-retrieved columnar ozone and/or precursor data, those machine-learning methods have significantly improved estimation accuracies (e.g., validated R^2 values higher than 0.80) and refined the spatial resolution of the estimates (e.g., 0.1°× 0.1° and 0.05°×0.05°) (Zhang et al., 2020; Mu et al., 2023b; Li and Cheng, 2021; Li et al., 2020; Mu et al., 2023a; Zhu et al., 2022; Xue et al., 2020; Chen et al., 2021). Given that the variation in ground-level ozone is influenced by atmospheric and geographic factors (Wang et al., 2022b; Tu et al., 2007; Zhu et al., 2022; Li et al., 2019; Fu and Tai, 2015), several studies have employed statistical and machine-learning algorithms using atmospheric components (e.g., $PM_{2.5}$), and meteorological factors (e.g., temperature, wind, sunshine, and precipitation), along with relatively high-resolution surface conditions (e.g., elevation and land cover) data, as predictors for modeling. While previous studies have estimated ground-level ozone concentrations across China with improved estimation performance (Ma et al., 2022a; Liu et al., 2020; Zhan et al., 2018; Chen et al., 2021; Wei et al., 2022; Shang et al., 2024), at least two key limitations persist: (1) despite advancements in resolution, these studies have not achieved high resolution in both spatial and temporal dimensions, such as daily 1-km estimates. This shortfall is partly due to the limited incorporation of suitable high-resolution spatiotemporal proxies into the models, which are essential for capturing fine-scale ozone gradients across space and time; (2) Although gap-free ozone estimates have been provided, few studies track long-term variations before 2005, and even fewer offer external or independent validation for pre-2013 estimates when national air quality monitoring data were

unavailable. Consequently, the current datasets are insufficiently detailed or validated to detect fine-scale intra- and inter-city ozone variations over time, thereby limiting the accuracy of exposure assessments.

Ozone is a short-lived pollutant, exhibiting significant spatial and temporal variations even over small areas and short periods (Mukherjee et al., 2018; Shi et al., 2023). The scarcity of long-term, spatiotemporally detailed ozone data has historically confined ozone research to identifying exposure hotspots and events from a broad-scale or a time-aggregated perspective (Liu et al., 2022; Mashat et al., 2020; Xia et al., 2022). The detailed intra-urban differences and short-duration phenomena over the past two decades remain largely unexplored. To address this gap, our study utilizes a long-term ground-level ozone concentration dataset across China from 2000 to 2020 with daily, 0.01° (~1 km) spatiotemporal resolution. This dataset is used to evaluate general spatial patterns of long-term ozone variations, identify hotspots of population exposure to ground-level ozone across multiple spatial and temporal scales, and examine the implications for mitigation policies and public health. The ozone dataset is estimated using our previously developed spatiotemporal high-resolution machine learning-based ozone estimation framework, which incorporates land surface temperature (LST), derived from long-term, high-resolution satellite remote sensing observations, as a primary predictor (He et al., 2024). To ensure the reliability of the long-term exposure analysis, the estimates were evaluated through rigorous cross-validation and independently validated using external ozone measurements. The exposure analysis integrates these high-resolution ozone estimates with detailed population distributions derived from geographic big data.

2 Data and Methodology

2.1 Long-term ozone estimates and validation

The present study builds on our previously developed high-resolution ozone modeling framework to hindcast long-term ozone concentration data across China from 2000 to 2020. That framework was designed to predict the daily maximum 8-hour average (MDA8) ozone concentrations at a 0.01° spatiotemporal resolution using the extreme gradient boosting (XGBoost) algorithm. It incorporated four groups of predictors: meteorological parameters (e.g., land surface temperature (LST), boundary layer height), pollutant variables (e.g., nitrogen dioxide, aerosol optical depth), geographical covariates (e.g., elevation, land cover classification), and temporal dummy variables (e.g., day of the year). In that model, satellite-derived LST data, with full coverage and daily, 0.01° resolution, served as the primary predictor. Since the data sources, preprocessing approaches, and predictor selection for the current long-term hindcast estimation model closely follow the previously developed modeling framework, further details are documented in Text S1.

The model development process closely mirrors that of our previous high-resolution model. The XGBoost algorithm (Chen and Guestrin, 2016) is also utilized to train the long-term hindcast model due to its demonstrated effectiveness in ground-level ozone estimation at an acceptable computational cost, as indicated by our previous study (Li et al., 2024b). Given that the Chinese National Air Quality Monitoring Network (NAQMN) was not established before 2013 and monitoring data from that period is unavailable, we apply a widely-used pre-2013 $PM_{2.5}$ hindcast modeling approach to predict long-term ozone concentrations (Ma et al., 2022b). Specifically, we train the ozone estimation model on data from 2014 to 2020, and once the

model is adequately trained, we apply it to retrospectively predict ozone concentrations for the past two decades, including the 14 years preceding the establishment of the NAQMN. The study period is partitioned following the approach of a previous study (Zhu et al., 2022), with 2014-2020 as the training period and 2000-2013 as the hindcast period. We exclude the year 2013 from our hindcast modeling due to the limited number and data quality of air quality monitoring stations during NAQMN's inaugural year. We focus on optimizing four critical hyperparameters of XGBoost to balance model performance and computational efficiency: (1) n_estimators, the number of trees in the model; (2) max_depth, which controls the maximum tree depth to prevent overfitting; (3) colsample_bytree, the proportion of features sampled for each tree; and (4) min_child_weight, the minimum number of samples required in a child node. We employ a random search with cross-validation to find the optimal settings for these hyperparameters, which are set at 400, 14, 0.8, and 4, respectively. This hyperparameter setting is a tradeoff between model performance and the computational demand. We implemented the modeling process in Python (ver. 3.9) with the Sklearn XGBoost package (ver. 1.7.3).

Due to the absence of nationwide ground-level ozone measurements prior to 2013, directly assessing the estimates for those years is challenging. To address this, we employ the leave-one-year-out cross-validation (CV) method to evaluate the reliability of our long-term hindcast model in estimating years without ground-level ozone measurements. This approach involves withholding data from one entire year during model training, simulating a hindcast scenario where ozone measurements are unavailable. This state-of-the-art evaluation technique is widely used in $PM_{2.5}$ hindcast modeling for pre-2013 predictions (Ma et al., 2022b). Additionally, although limited, some ground-level ozone measurements from before 2013 are available from monitoring sites in Hong Kong. To further validate the pre-2013 predictions, we use these independent Hong Kong ozone measurements—excluded from model development—to directly assess the model's performance during the extended historical period. This provides a more straightforward evaluation, given the lack of nationwide pre-2013 ozone data. In addition to validating hindcast predictions for the pre-2013 period, we also apply the random 10-fold CV to assess the overall performance of our model. This process involves randomly dividing the sample dataset into 10 subsets, using nine subsets to train the model and the remaining subset to test it. This procedure is repeated 10 times to ensure that each daily MDA8 measurement has a corresponding estimate for comparison. The site- and day-based CVs specifically assess the model's spatial and temporal performance. We compute several statistical metrics, including R^2, RMSE (Root-Mean-Squared Error), and MAE (Mean Absolute Error), to compare the MDA8 measurements with the model estimates.

2.2 Multi-scale spatiotemporal analysis

We generated full-coverage, daily 1-km resolution ozone estimates across China from 2000 to 2020 using the proposed hindcast machine-learning method. Based on these long-term, high-resolution spatiotemporal estimates, we analyzed interannual, seasonal, and monthly variations, as well as short-term exposure characteristics, at national, regional, county, and pixel scales. Particular attention was given to typical high-exposure regions, which were identified by mapping the spatial distributions of seasonal averages across the study areas over the past two decades.

2.2.1 Long-term trend analysis

To assess long-term exposure trends, we combined the MDA8 ozone estimates with concurrent yearly 1-km LandScan population distributions (Rose et al., 2020) to compute the annual and seasonal population-weighted mean MDA8 ozone concentrations for China and typical regional hotspots from 2000 to 2020. These population-weighted concentrations were used to analyze interannual variations, seasonal fluctuations, and regional differences in long-term ozone trends at both national and regional levels. The four seasons were defined as follows: spring (March-May), summer (June-August), autumn (September-November), and winter (December-February). The detailed formulation for calculating population-weighted ozone levels (O_3_POP) for a given region is presented in (Eq. 1). The long-term linear trend was estimated using the least-squares approach, consistent with previous studies (Li et al., 2019; He et al., 2016).

$$O_3\text{\_POP} = \sum(\text{POP}_i \times O_{3_i}) \Big/ \sum \text{POP}_i \quad \text{(Eq. 1)}$$

where is POP_i and O_{3_i} denote the population and the estimated MDA8 O_3 level in grid cell i.

2.2.2 Monthly pattern analysis

We calculated the monthly population-weighted mean MDA8 ozone concentrations from 2000 to 2020 and identified the peak and trough values from these monthly time series. To capture both seasonal extremes and the underlying background ozone concentrations, we calculated linear trends separately for the peaks and troughs. Additionally, we applied a Mann-Kendall test to the monthly peak time series to determine whether there is a statistically significant trend in maximum ozone concentrations over the two decades for various regions in China. To assess the extent of severe ozone pollution across counties over time, we generated time series data on the number of counties with monthly ozone concentrations exceeding 100 μg/m^3 and analyzed the linear trend. The threshold of 100 μg/m^3 was selected based on the Chinese National Air Quality Standard Level 2 and the WHO (World Health Organization) air quality guideline as an indicator of severe exposure. From the monthly exposure time series, we selected a month with severe ozone pollution to map the spatial disparity in ozone exposure at the county level.

2.2.3 Short-term characteristics analysis

By overlaying the daily ozone estimates with 1-km LandScan population maps, we calculated the number of people exposed to different ozone concentration levels. Our primary focus was on two key thresholds: 100 μg/m^3, the 8-hour air quality guideline recommended by the WHO, and 160 μg/m^3, the Level 2 standard set by the Chinese National Air Quality Standard. Additionally, we generated a high-exposure risk map for extremely severe ozone pollution by showing the spatial distribution of the percentage of days with ozone concentrations exceeding 160 μg/m^3, the second level of the national air quality standard.

Table 1. The random 10-fold CV results for the proposed long-term MDA8 O_3 modeling method.

Period	Sample size	Daily					Monthly				
		R^2	Slope	Intercept	RMSE ($\mu g/m^3$)	MAE ($\mu g/m^3$)	R^2	Slope	Intercept	RMSE ($\mu g/m^3$)	MAE ($\mu g/m^3$)
All	3,249,653	0.83	0.81	17.74	18.89	13.71	0.96	0.91	8.22	7.15	5.12
2014	292,643	0.76	0.75	23.70	24.03	17.00	0.94	0.88	12.43	9.85	7.08
2015	476,631	0.78	0.77	21.20	21.35	15.51	0.94	0.88	11.70	9.01	6.65
2016	466,618	0.79	0.78	20.25	20.37	14.92	0.95	0.89	9.92	8.14	6.03
2017	498,439	0.84	0.83	16.92	18.61	13.76	0.96	0.92	6.96	6.83	5.10
2018	496,152	0.84	0.82	16.78	17.89	13.24	0.97	0.93	6.43	6.07	4.59
2019	498,544	0.87	0.86	13.63	16.56	12.30	0.98	0.95	4.85	5.36	3.95
2020	520,626	0.87	0.87	12.59	14.67	10.86	0.98	0.96	4.13	4.28	3.19

3 Results

3.1 Evaluation results of model performance and predictions

3.1.1 Validation of overall model performance

Table 1 presents the random 10-fold CV results of our proposed method, showing that our MDA8 estimates closely align with the measured MDA8 O_3 concentrations. For the CV over the entire modeling period, the R^2 values for daily and monthly MDA8 estimates were 0.83 and 0.96, respectively. The corresponding RMSE (MAE) values were 18.89 $\mu g/m^3$ (13.71 $\mu g/m^3$) for daily estimates and 7.15 $\mu g/m^3$ (5.12 $\mu g/m^3$) for monthly estimates. We further compiled the CV results by province, and the XGBoost model excelled in Beijing, Tianjin, Hebei, Shanxi, and Henan provinces/cities, achieving CV R^2 values above 0.86, but it performed less well in Fujian and Taiwan, where R^2 values were below 0.70 (Fig. S3). When examined by year, the R^2 [RMSE] values improved from 0.76 [24.03 $\mu g/m^3$] in 2014 to 0.87 [14.67 $\mu g/m^3$] in 2020. This improvement is primarily attributed to the increased sample size resulting from the addition of more monitoring stations in later years. Additionally, the estimation accuracy metrics at the monthly level were significantly better than those at the daily level, suggesting that temporal averaging can mitigate the uncertainty in model estimates. Overall, focusing on estimation accuracy, our proposed method achieves performance that is superior to, or at least comparable with, previous ozone modeling studies, with sample-based 10-fold CV R^2 values at the daily level ranging from 0.70 to 0.87 (Table S4) (Ma et al., 2022a; Liu et al., 2020; Xue et al., 2020; Zhu et al., 2022; Chen et al., 2021; Wei et al., 2022).

3.1.2 Evaluation of pre-2013 estimates

We employed a rigorous validation approach, namely the leave-one-year-out CV, to assess the model's predictive capability in years lacking national ground-level O_3 monitoring data. Figure 1a illustrates that our proposed modeling framework predicts historical O_3 data with somewhat high estimation uncertainty at the daily level (i.e., R^2=0.57, RMSE=29.72 $\mu g/m^3$, MPE=22.11 $\mu g/m^3$) and reduced uncertainties at the monthly level (i.e., R^2=0.74 and RMSE=17.75 $\mu g/m^3$, MPE=12.76 $\mu g/m^3$). Additionally, an independent evaluation using 17,122 ozone measurements from Hong Kong, spanning 2005 to 2012, demonstrates that our model achieved R^2 values ranging from 0.31 to 0.59 and RMSE values from 34.65 to 45.40 $\mu g/m^3$, with averages of 0.41 and 41.95 $\mu g/m^3$, respectively (Fig. 1b and Table S5). These results are comparable to those from the leave-one-year-out CV conducted over Hong Kong (i.e., R^2 of 0.44, RMSE of 32.84 $\mu g/m^3$, MPE=24.86 $\mu g/m^3$ in Table S6). This consistency underscores that the reliability of the leave-one-year-out CV for assessing model's predictive performance in periods without national ground-level ozone measurements.

While several studies have developed long-term O_3 estimation models for China, few have quantitatively evaluated the predictive accuracy of their pre-2013 estimates (Table S4). (Liu et al., 2020; Ma et al., 2022a) reported that these models predicted pre-2013 MDA8 O_3 concentrations with leave-one-year-out CV R^2 [RMSE] of 0.69 [19.47 $\mu g/m^3$] and day-based 10-fold CV R^2 of 0.63 at the monthly level, respectively. Compared with these earlier long-term ozone modeling studies (Table S4), our results demonstrate more reliable for historical years without ground-level ozone measurements, with stronger leave-one-year-out CV and day-based 10-fold CV results, particularly at the aggregated monthly level (Chen et al., 2021; Liu et al., 2020; Ma et al., 2022a; Xue et al., 2020; Zhu et al., 2022; Wei et al., 2022). These findings indicate that our model not only captures long-term trends but also the fine-scale variations in ozone across China more accurately, making it valuable for both long-term and short-term ozone variation and exposure research.

3.1.3 Estimated high-resolution maps of ground-level ozone

We selected a subset from June 2018, identified as a hotspot for high ozone levels based on ground-level monitoring data, from our long-term, full-coverage MDA8 O_3 estimates generated by the proposed modeling framework. This subset was used to evaluate whether the extrapolated surfaces accurately capture day-to-day and fine-scale variations in ground-level ozone concentrations. Figure 2 (a-d) presents a comparison of monthly mean ground-level MDA8 O_3 concentrations from our high-resolution estimates with the 10-km MDA8 estimates by (Wei et al., 2022) and in-situ measurements for June 2018 — a month noted for high ozone concentrations at the monitoring stations. The nationwide distributions illustrate that our model successfully captures the general spatial variation pattern of ground-level ozone across China, aligning well with both (Wei et al., 2022)'s findings and measured values (Fig. 2a). Zoom-in maps of Jinan, Wuhan, and Chongqing highlight that our modeling approach predicts fine-structures in ground-level ozone concentrations that are not discernible in coarser-resolution maps and in-situ measurements (Fig. 2 b-d). Additionally, comparisons of daily time series of MDA8 O_3 estimates versus observations in 2018 (Fig. 2d & Fig. S4) show that our method effectively captures daily and seasonal variability, although it tends to underestimate extremely high concentrations. This underestimation is likely due to the regression approach, which

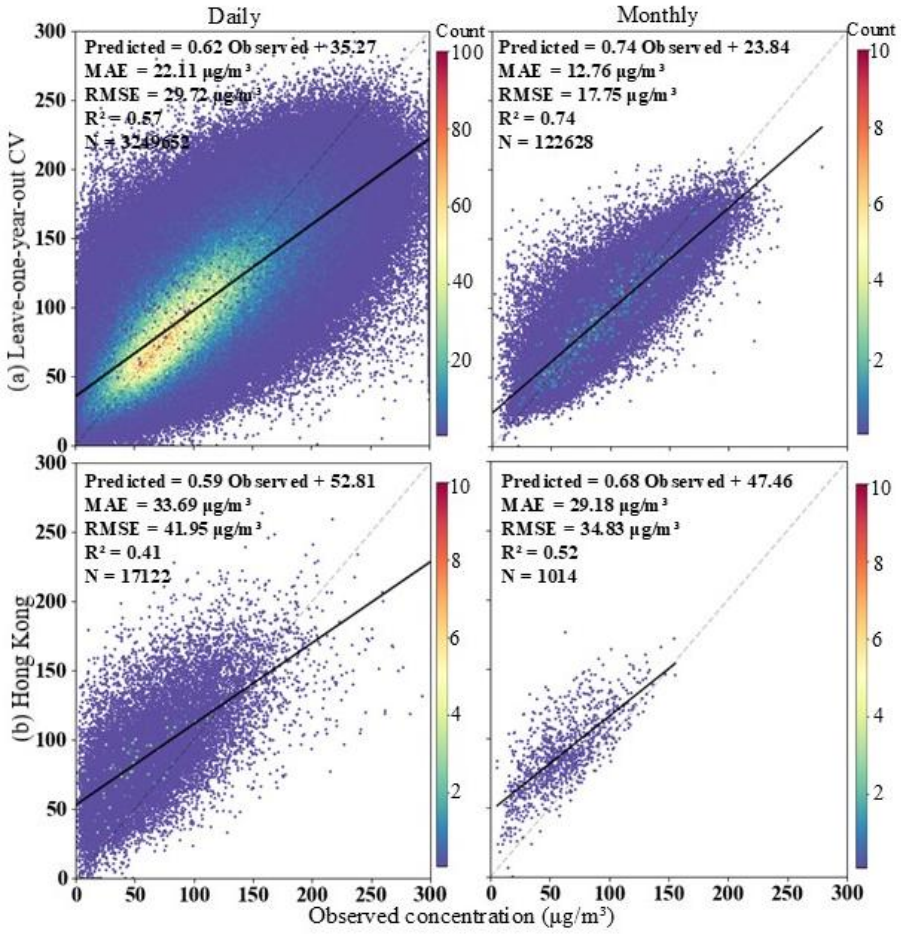

Figure 1. Validation results of historical MDA8 O_3 estimates: (a) leave-one-year-out CV at daily and monthly levels; (b) independent validation results against monitoring data from Hong Kong from 2005 to 2012, where the monitoring data over Hong Kong have not been employed in model development.

optimizes predictions based on average behavior. Overall, while 10-km and in-situ data primarily identify broad 'hotspots' of ground-level ozone (e.g., at the city scale), our high-resolution predictions uncover much more intricate structures, capturing sharp spatial and temporal gradients shaped by both natural and anthropogenic factors.

3.2 Spatial distribution and long-term trend of ground-level O_3 exposure

Figure 3a illustrates how long-term pollution hotspots vary by region and season. In spring, moderate O_3 pollution widespread in the eastern region, with most MDA8 O_3 concentrations ranging between 110 μg/m^3 and 130 μg/m^3, except in the southern provinces. Summer sees severe ozone pollution, with concentrations exceeding 100 μg/m^3 in most areas, apart from the Qinghai-Tibet plateau and Yunnan province. During this season, the central North China Plain (NCP) experiences the high-

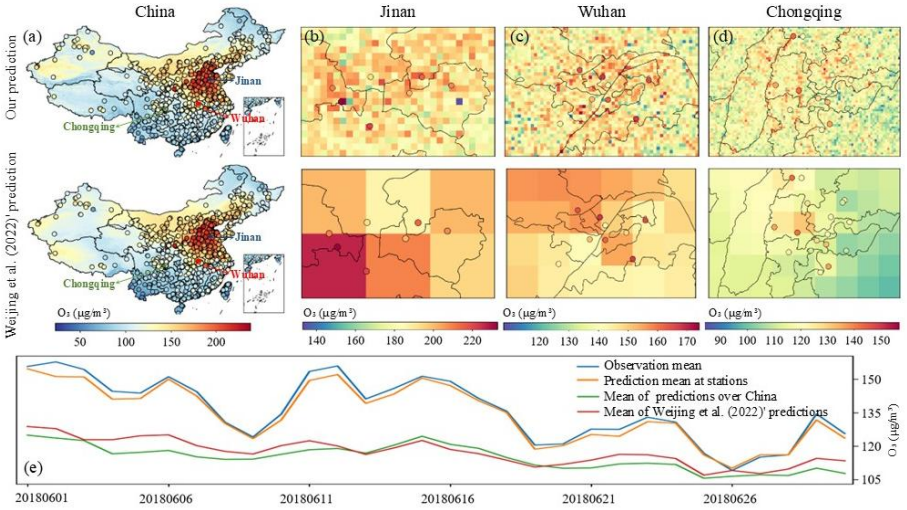

Figure 2. Spatiotemporal comparisons of ground-level ozone predictions vs. observations in China in June 2018: (a) monthly mean map of MDA8 O_3 predictions with station ozone measurements (monthly valid measurements for each station >15); zoom-in maps over (b) Jinan, (c) Wuhan, and (d) Chongqing; (e) Time series of mean MDA8 O_3 concentrations over China during June 2018.

est polluted levels, with 21-year mean MDA8 O_3 concentrations routinely surpassing 140 $\mu g/m^3$. In autumn, the southern provinces experience mild ozone pollution with most MDA8 O_3 levels between 100 $\mu g/m^3$ and 110 $\mu g/m^3$, while the Pearl River Delta (PRD) becomes the prominent ozone exposure hotspot, with most concentrations exceeding 120 $\mu g/m^3$. Winter features the lowest ozone levels, with nearly all regions recording MDA8 O_3 concentrations below 100 $\mu g/m^3$. Consequently, we identified eastern China, the NCP, and the PRD as long-term ozone high-exposure regions, which were given special attention in the subsequent analysis.

By integrating yearly population distributions from Landscan (Rose et al., 2020), we analyzed the spatiotemporal patterns of exposure to ground-level ozone across China over the past two decades. Figure 3 (b-c) shows the annual and seasonal trends of population-weighted mean MDA8 O_3 concentrations, revealing long-term trends that are non-monotonous and vary significantly across different regions. As illustrated in the annual exposure time series (Fig. 3b), two turning points are observed around 2008 and 2015: in the first phase of 2001-2007, the population-weighted exposure to ozone increased with a linear slope of 0.47 $\mu g/m^3$/year, then decreased post-2008 with a slope of -0.58 $\mu g/m^3$/year, followed by a substantial rise at a rate of 1.16 $\mu g/m^3$/year during the third phase of 2016-2020. These shifting exposure trajectories also displayed pronounced seasonal and regional variations (Fig. 3c). During the 2001-2007 phase, eastern China and the NCP experienced a significant rise in ozone exposure during the summer months, with slopes ranging from 1.39 to 1.91 $\mu g/m^3$/year, whereas the PRD region saw its most substantial increases in autumn, with a notable slope of 3.84 $\mu g/m^3$/year. In the second phase, the three typical ozone hotpots generally showed decreasing trends across all seasons (slopes from -0.03 to -1.02 $\mu g/m^3$/year), except for a slight increase during the summer in the NCP (slope of 0.64 $\mu g/m^3$/year). Moving into the 2016-2020 phase, these typical hotspots transitioned to marked increasing trends in autumn, particularly in the PRD, which displayed a steep increase with a slope of

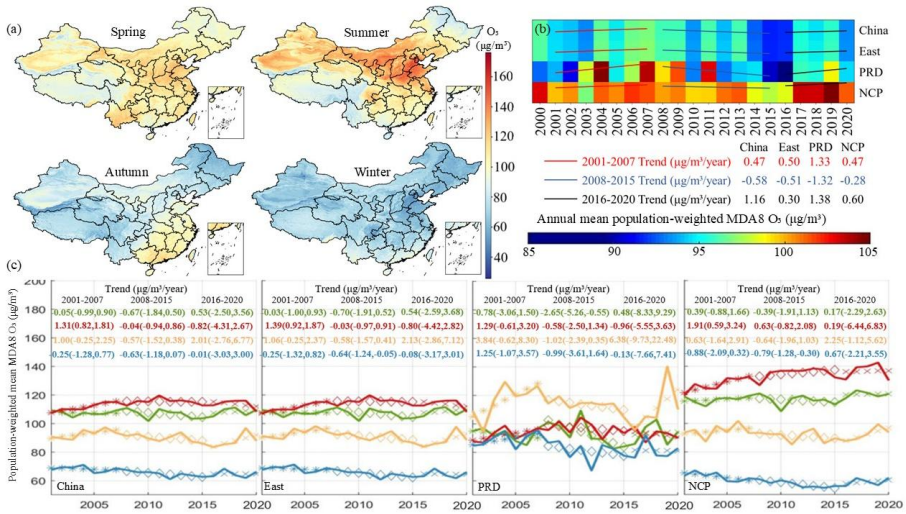

Figure 3. Overall spatiotemporal patterns of exposure to ground-level ozone in China over the past two decades: (a) Spatial map of seasonal mean MDA8 O_3 concentrations during 2000-2020; (b) annual mean population-weighted MDA8 O_3 concentrations over China and the three regions (i.e., eastern China, PRD, and NCP); (c) Seasonal population-weighted mean MDA8 O_3 concentrations over China and three typical regions, and their linear trends (green for spring, red for summer, orange for autumn, and blue for winter), where asterisks (*), diamonds (◊), and crosses (x) correspond to the linear trends in the 2001–2007, 2008–2015, and 2016–2020 sub-periods, with 95% confidence intervals and colors matched to seasons.

6.38 μg/m^3/year. Conversely, while other regions exhibited declining trends during the summer season of this phase, the NCP continued to show an upward trend with a slope of 0.19 μg/m^3/year.

3.3 Monthly exposure and county-level pattern

To investigate how the most severe ozone pollution events and baseline levels have evolved over time, we further analyzed monthly exposure patterns, focusing specifically on the trends in monthly population-weighted mean MDA8 ozone concentration peaks and troughs across China and three key regions. Overall, the monthly ozone concentrations followed a three-phase trend, similar to the annual patterns identified earlier (as shown in Fig. S5 and Fig. 3b), with slight regional variations in the slopes. However, a closer examination of the monthly peaks and troughs revealed distinct changes. As indicated in Fig. 4a, all regions experienced an increase during the first phase, with the PRD recording a notable rise at a rate of 4.37 μg/m^3/year. The second phase showed general declines across most regions (slopes range from -0.99 to -1.19 μg/m^3/year), except for the PRD (slope=-0.009 μg/m^3/year), which remained relatively stable. The subsequent phase again saw increases in all regions, ranging from 0.19 to 0.44 μg/m^3/year, with the PRD experiencing a significant uptick at a slope of 3.19 μg/m^3/year. The trends in monthly troughs mirrored the decline observed in the second phase, albeit with varied patterns in other stages. From 2001 to 2007, both China and eastern China registered slight increases, whereas the NCP and PRD noted decreases in trough levels. During the 2016-2020 period, the PRD showed a marked increase, with a slope of 2.81 μg/m^3/year, contrasting with decreases

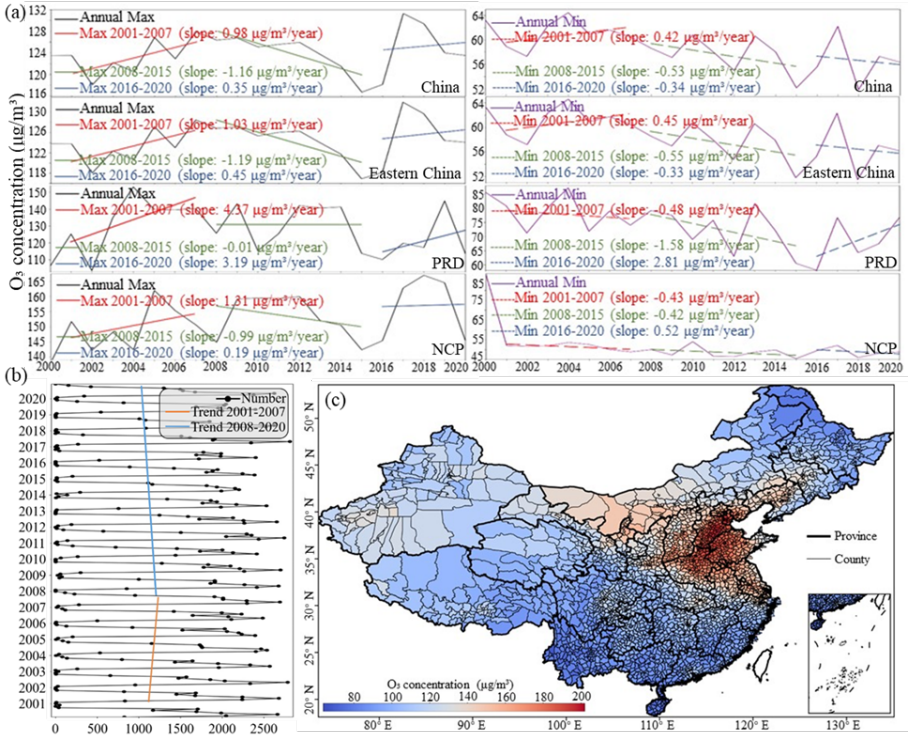

Figure 4. Spatiotemporal distributions of monthly population-weighted mean MDA8 O_3 concentrations over China and the three typical regions: (a) time series with three-piece trend lines of peaks (left panel) and troughs (right panel) from 2001 to 2020; (b) number of counties with monthly ozone concentrations exceeding 100 μg/m^3 from 2000 to 2020; (c) spatial distribution of county-level mean concentrations in June 2018.

ranging from -0.33 to -0.52 μg/m^3/year in the other regions. Additionally, over the past two decades, the monthly peaks predominantly occurred in June. However, results from the Mann-Kendall test (Table S7) indicate a significant shift in the timing of peak ozone concentrations across most of China, with p-values below 0.05 for China, the east, and the NCP, suggesting a potential shift from June to earlier in May in recent years.

To provide a spatial and temporal overview of severe ozone pollution trends across counties in China, we tracked the number of counties where monthly ozone concentrations exceeded 100 μg/m^3 from 2000 to 2020. As shown in Fig. 4b, the trend exhibits significant seasonal variation each year, with peaks typically occurring in late spring and early fall. While the seasonal pattern remains consistent annually, the amplitude of these peaks fluctuates from year to year. Notably, in May 2017, 2,812 counties exceeded the ozone threshold, compared to an average of 2,543 counties during the month of May in other years. On average, 1,142 of the 2,900 counties exceeded this 100 μg/m^3 threshold monthly, with the 25th and 75th percentiles at 38 and 2,002 counties, respectively. Interestingly, the time series for the number of counties with exceedances did not exhibit the three-phase variation identified earlier. Instead, the number of counties exceeding the threshold increased from 2001 to ~2007, with a slope of 16.84 per year, and then decreased in the subsequent years, with a slope of -12.44 per year.

Figure 4c displays a county-level spatial map from June 2018, a month identified as a hotspot for high ozone levels, highlighting significant spatial disparities in ozone exposure within cities. For example, in Beijing, the population-weighted mean MDA8 O_3 concentrations ranged from 141.23 μg/m^3 in Yanqing in the northwest to 180.33 μg/m^3 in Tongzhou in the southeast. Nationally, the highest exposure levels were recorded in Xiqing and Beichen counties in Tianjin, with concentrations around 200 μg/m^3. Conversely, the lowest exposures were observed in two southwestern counties in Yunnan province and three southeastern counties in Hainan province, with concentrations below 70 μg/m^3.

3.4 Short-term exposure characteristics and extreme episodes of ground-level O_3

We observed the day-to-day variation in ground-level ozone concentrations for China as a whole and for the three typical regions over the past two decades. The coefficient of variation of the daily MDA8 O_3 predictions indicates significant spatial heterogeneity in the nationwide distribution of ambient ozone, with values ranging from 0.16 to 0.41 (Fig. S6). This variability is characterized by notable seasonality, displaying the highest mean values in autumn (0.29) and the lowest in spring (0.22).

Overlaying daily MDA8 O_3 predictions with population distribution, Fig. 5a reveals that from March 2000 to December 2020, over 60% of the Chinese population was exposed to MDA8 O_3 concentrations exceeding 100 μg/m^3, defined as the first level of the national ambient air quality standard, on more than 31% of the total prediction days. The long-term variation of these exposure ratios follows a three-piece pattern (Fig. S7) similar to the annual ozone exposure trend identified in Section 3.2. The highest exposure months are May and June, with daily ratios around 70%. Particularly in May 2007 and 2017, the average ratio reached 79%, with ranging between 56% and 97%. At the regional level, daily ozone exposure in the three typical ozone exposure hotspots was more severe than the national average, especially for the NCP and PRD regions. In these regions, ~60% and ~40% of days, respectively, saw the population exposed to ozone levels above 100 μg/m^3. Furthermore, ~5% of days in the NCP and ~2% in the PRD exceeded the national second-level limit of 160 μg/m^3 (Fig. 5b). The spatial map in Fig. 5c further illustrates that extremely severe ozone exposure was concentrated in the NCP region, especially for the central NCP, with most area experiencing more than 10% of days with concentration exceeding 160 μg/m^3. Over time, this severe exposure expanded from part of south Hebei, Tianjin, north Henan, and west Shandong in the first phase of 2001-2007 to cover most of the NCP region in the third phase of 2016-2020.

The severe ozone pollution events are usually associated with meteorological conditions (Yang et al., 2024). Figure 6 exemplified an extreme ozone pollution episode on 25 June-5 July of 2017 over the NCP. The West Pacific Subtropical High, positioned between 20–26°N, significantly influenced ozone distribution over the Yangtze River Delta by modulating precipitation and solar radiation. High relative humidity in the region suppressed ozone formation in this region, resulting in lower concentrations. In contrast, the Beijing-Tianjin-Hebei and its surrounding area (BTH) experienced favorable conditions for ozone production under an anomalous high-pressure system in the upper troposphere (Xu et al., 2019). Warm, southerly winds in the lower troposphere contributed to higher temperatures and northward transport of aged air masses, increasing ozone and its precursors. Furthermore, a persistent temperature inversion in the BTH trapped pollutants in lower layers, exacerbating ozone pollution. This inversion preserved ozone at night and facilitated its descent to the surface at sunrise, worsening the pollution. These persistent conditions sustained severe regional ozone pollution events in the BTH (Mao et al., 2020).

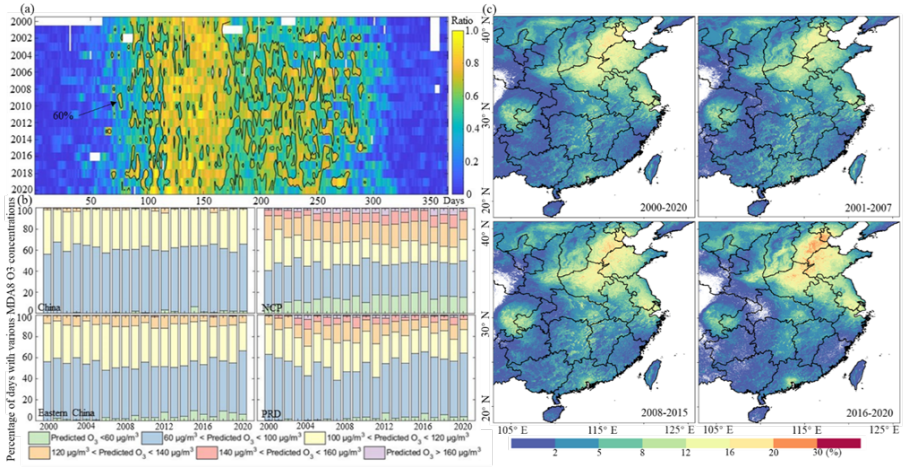

Figure 5. Day-to-day patterns of ground-level ozone exposure levels from 2000 to 2020: (a) heatmap of daily ratios of the population exposed to MDA8 O_3 concentration exceeding 100 $\mu g/m^3$; (b) percentage of days with various MDA8 O_3 concentrations; and (c) high-exposure risk maps calculated for 2000-2020 and the three phases.

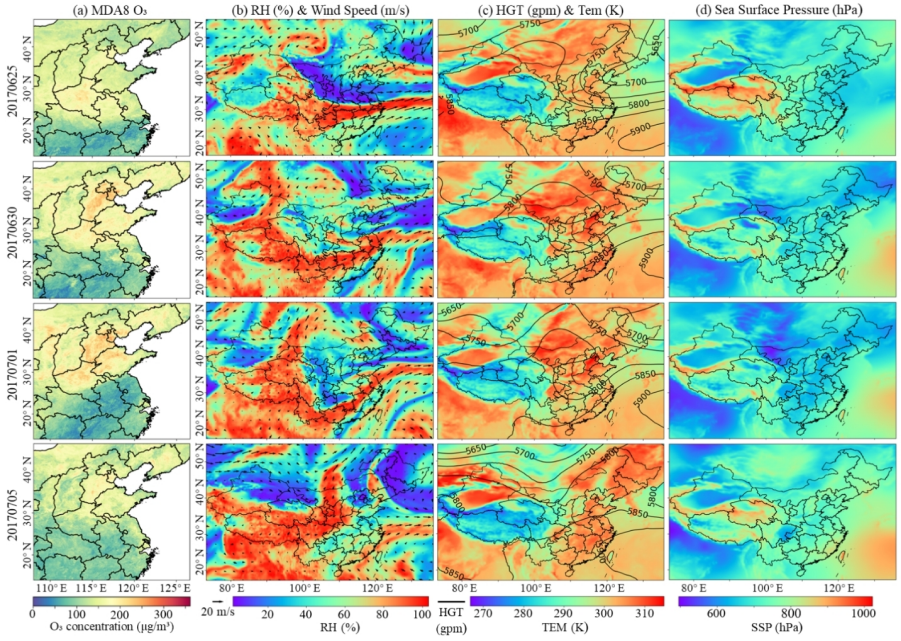

Figure 6. Spatial distributions of daily MDA8 O_3 and meteorological fields (relative humidity (RH), wind speed (WS) at 500 hPa, geopotential height field (HGT) at 500 hPa, air temperature (T) at 2m, and sea surface pressure (SSP) in 25 June -5 July 2017.

4 Discussion

In this study, we developed an XGBoost-based prediction model to hindcast long-term, full-coverage ground-level MDA8 O_3 concentrations across China with daily and 1-km spatiotemporal resolution. To the best of our knowledge, our model's performance, with a sample-based 10-fold CV R^2 of 0.83 at the daily level, is comparable to other national-scale ozone modeling studies in China, which have reported validation R^2 values ranging from 0.77 to 0.87 (Table S4). Despite similar performance levels, our modeling framework offers superior spatiotemporal resolution (daily and 1-km vs. monthly or 0.05° or coarser) and covers a longer prediction period (2000-2020 vs. 2005-2019 or shorter) compared to these studies. The rigorous hindcast and individual validation results confirm that our long-term estimates reasonably represent day-to-day trends and intra-urban variations in ground-level ozone, including for the pre-2013 period. The long-term, full-coverage estimates capture short-term local pollution variations and details not revealed by previously coarser resolution or shorter-period data (Fig. 1 and 3). For example, Fig. S8 illustrates a case study from Wuhan on May 28 2017, a day characterized by elevated ozone levels, showing local NO_2 levels titrated O_3, resulting in observed ozone concentrations that are lower than those downwind. Consistent with our previous findings (He et al., 2024), incorporating LST—closely linked to ozone variations and available at high spatiotemporal resolutions—significantly enhances the overall quality of our estimation data. This improvement is demonstrated by its leading rank in variable importance (Fig. S9) and the observed increase in R^2 values by 0.04–0.06 across sample-, site-, and day-based 10-fold CVs when comparing models with and without LST (Table S8). Additionally, its critical role in hindcasting ground-level ozone estimates for the pre-2013 unmonitored period is validated through improvements in estimation accuracy, as reflected by an R^2 increase of 0.07 in the leave-one-year-out CV (Table S8) and 0.02 in independent validation using Hong Kong in-situ measurements (Table S9). Additionally, the inclusion of other spatiotemporal covariates related to ozone formation and dispersion, such as radiation, terrain, and the ozone precursor NO_2, helps the model capture the complex spatiotemporal dynamics of ground-level ozone.

Our long-term trend analysis reveals a three-phase variation pattern in ground-level ozone across China over the past two decades, characterized by significant seasonality and region disparities (Fig. 3, Fig. S5, Fig. 4). This pattern likely results from a complex interplay of environmental, regulatory, and climatic factors influencing ozone levels. Similar to long-term $PM_{2.5}$ in China (He et al., 2023), the first 2001-2007 phase presented an increasing trend, possibly linked to rapid industrial growth and urbanization accompanied by lenient environmental controls. This period likely saw higher emissions of ozone precursors such as volatile organic compounds (VOCs) and nitrogen oxides (NOx) (Akimoto, 2003; Ahammed et al., 2006). In contrast, the second phase featured a general decline in ozone levels, coinciding with stricter air quality policies implemented by the central government, which included notable reductions in nitrate emissions observed during 2012-2016 (Wang et al., 2019). However, unlike $PM_{2.5}$, which experienced a marked decrease after 2013, ground-level ozone entered a third phase (2016–2020) of substantial increase. This divergence can be partly attributed to the decline in $PM_{2.5}$ levels, which likely slowed the removal of hydroperoxy radicals, thereby enhancing ozone production (Li et al., 2019). These findings highlight the critical need for integrated control of ozone and $PM_{2.5}$ pollution to avoid unintended trade-offs between these pollutants.

Our ozone exposure analysis identified several hotspots, with the most severe exposures—concentrations exceeding 160 $\mu g/m^3$—primarily observed in the NCP. This region has experienced an increasing trend in both the geographical extent and frequency of these high concentrations (Fig. 5). Temporally, we observed a notable shift in the peak ozone exposure month from June to May, especially pronounced in the NCP. This escalation in ozone pollution levels and the earlier annual peak may be attributed to changes in meteorological conditions, such as extreme high temperatures (Wang et al., 2022a), and air pollutant emissions, notably the reduction in NOx emissions coupled with high emissions of VOCs (Ke et al., 2021), which are conducive to ozone formation. Furthermore, the significant reduction in ambient particulate matters in the NCP in recent years has also contributed to worsening ozone conditions in this region (Li and Li, 2023). These shifts in spatial and temporal exposure hotspots should raise significant concern for both central and local governments, as the expanding extent and prolonged duration of high ozone levels could exacerbate public health risks and broadly impact agricultural productivity. Furthermore, the distribution of ozone exposure hotspots presents significant seasonal changes, with summertime hotspots predominantly occurring in the NCP and shifting to the PRD during autumn (Fig. 3). These differing trends highlight the critical role of regional weather patterns in shaping ozone dynamics. As a result, policy measures should be carefully tailored to address not only the unique needs of specific regions but also the seasons during which ozone peaks are most pronounced, ensuring more effective and targeted mitigation strategies.

Based on the high-resolution estimates, we quantitatively identified counties with the highest and lowest ozone levels (Fig. 4b-c), offering critical insights to inform resource allocation and targeted pollution control measures. For instance, counties such as Xiqing and Beichen in Tianjin, identified as having high ozone levels, can be prioritized for implementing targeted emission control policies and public health campaigns to mitigate health risks for local residents. These localized insights are often overlooked in broader-scale regional analyses. Previous studies relying on coarser-resolution data have typically focused on large urban agglomerations, such as the Beijing-Tianjin-Hebei region and the Pearl River Delta (PRD) (Wei et al., 2022), neglecting smaller yet critically affected areas. Conversely, while pixel-level analyses offer highly detailed spatial patterns, they may lack the administrative relevance needed for actionable policy decisions. By bridging the gap between regional and pixel-level analyses, our county-level analysis provides actionable and geographically specific recommendations, empowering policymakers to address ozone pollution more effectively.

The primary source of uncertainty in this study lies in the long-term ozone estimates. Since the NAQMN was not established before 2013, monitoring data from earlier years is unavailable. As a result, we could not directly train the model for that period. Instead, we applied the model developed for post-2014 data to hindcast ozone levels for the earlier unmonitored years. Consequently, the estimated ozone levels for these years may carry a certain degree of uncertainty, which could impact the spatiotemporal analysis. However, we conducted rigorous validation of the hindcast estimates, and the time-aggregated validation results demonstrated significant improvements in the accuracy of the pre-2013 estimates (R^2 of 0.74 at the monthly scale in Fig. 1). These findings suggest that the spatiotemporal exposure analysis, particularly regarding long-term variations, is robust and reliable.

5 Conclusions

In this study, we developed a multi-source, high-resolution modeling method using the XGBoost algorithm to hindcast long-term ground-level ozone concentrations across China. By utilizing this approach, we generated daily ozone estimates from 2000 to 2020, enabling the analysis of spatiotemporal exposure characteristics across multiple scales. The key findings of this study are summarized as follows:

(1) **Improved ozone hindcasting using satellite LST:** We successfully extended our high-resolution ozone modeling method by incorporating satellite-derived LST as a primary predictor. This enhancement improved the accuracy of hindcasting ozone concentrations over historically unmonitored periods. Comparative results confirmed that the inclusion of satellite LST significantly strengthens the model's long-term performance.

(2) **Non-monotonous long-term trends and seasonal shifts:** Our long-term analysis revealed a three-phase variation pattern in ground-level ozone levels over the past two decades, marked by regional and seasonal fluctuations. From 2001 to 2007, ozone concentrations increased at a rate of 0.47 μg/m^3/year, followed by a decline post-2008 at a rate of -0.58 μg/m^3/year, and a significant rise during 2016–2020 at a rate of 1.16 μg/m^3/year. Seasonal shifts were prominent, with high ozone levels concentrated in spring in eastern China, summer in the NCP, and autumn in the PRD. Notably, the PRD exhibited a sharp increase in autumn ozone levels during the third phase, with a rate of 6.38 μg/m^3/year.

(3) **Emerging exposure hotspots:** Our exposure analysis identified ozone concentrations exceeding 100 μg/m^3, which historically peaked in June but have shifted earlier to May in recent years. Additionally, dangerous exposure levels above 160 μg/m^3 were predominantly concentrated in the NCP, with an expanding trend in both extent and duration. Day-to-day analyses of ozone pollution episodes further underscored the role of meteorological conditions in driving extreme ozone events.

Overall, our rigorously validated estimates and exposure analyses provide critical data to inform environmental policy-making and public health research, laying the groundwork for targeted interventions to mitigate ozone exposure risks.

Data availability. The final ozone estimates will be available at https://doi.org/10.5281/zenodo.4569557.

Author contributions. QH designed the study framework, and conducted the formal analysis. JC, TY and WW processed the data, developed the code and validated the estimation model and visualized the results. The manuscript was initially written by QH and revised by PS, MZ, and JH.

Competing interests. At least one of the (co-)authors is a member of the editorial board of Atmospheric Chemistry and Physics.

Acknowledgements. This study is supported by the National Natural Science Foundation of China (Grant NO. 41901324, 42201369).

References

Ahammed, Y. N., Reddy, R. R., Gopal, K. R., and Narasimhulu, K.: Seasonal variation of the surface ozone and its precursor gases during 2001–2003, measured at Anantapur (14.62°N), a semi-arid site in India, Atmos. Res., Vol.80, 151-164, 10.1016/j.atmosres.2005.07.002, 2006.

Akimoto, H.: Global Air Quality and Pollution, Science, 302, 1716-1719, doi:10.1126/science.1092666, 2003.

Alexeeff, S. E., Ananya, R., Jun, S., Xi, L., Kyle, M., Apte, J. S., Christopher, P., Stephen, S., and Van, D. E. S. K.: High-resolution mapping of traffic related air pollution with Google street view cars and incidence of cardiovascular events within neighborhoods in Oakland, CA, Environ. Health, 17, 38, 2018.

Burnett, R. T., Dales, R. E., Raizenne, M. E., Krewski, D., Summers, P. W., Roberts, G. R., Raadyoung, M., Dann, T., and Brook, J.: Effects of Low Ambient Levels of Ozone and Sulfates on the Frequency of Respiratory Admissions to Ontario Hospitals, Environ. Res., Vol.65, 172-194, 10.1006/enrs.1994.1030, 1994.

Chen, G., Chen, J., Dong, G.-h., Yang, B.-y., Liu, Y., Lu, T., Yu, P., Guo, Y., and Li, S.: Improving satellite-based estimation of surface ozone across China during 2008-2019 using iterative random forest model and high-resolution grid meteorological data, Sustainable Cities Soc., Vol.69, 102807, 10.1016/j.scs.2021.102807, 2021.

Chen, T. and Guestrin, C.: XGBoost: A Scalable Tree Boosting System, ACM, 2016.

Chen, Y., Li, H., Karimian, H., Li, M., Fan, Q., and Xu, Z.: Spatio-temporal variation of ozone pollution risk and its influencing factors in China based on Geodetector and Geospatial models, Chemosphere, 302, 134843, 2022.

Dias, D. and Tchepel, O.: Spatial and Temporal Dynamics in Air Pollution Exposure Assessment, International Journal of Environmental Research & Public Health, Vol.15, 558, 10.3390/ijerph15030558, 2018.

Fiore, A., Jacob, D. J., Liu, H., Yantosca, R. M., Fairlie, T. D., and Li, Q.: Variability in surface ozone background over the United States: Implications for air quality policy, Journal of Geophysical Research:Atmospheres, Vol.108, 0, 10.1029/2003jd003855, 2003.

Fu, Y. and Tai, A.: Impact of climate and land cover changes on tropospheric ozone air quality and public health in East Asia between 1980 and 2010, Atmospheric Chemistry & Physics, Vol.15, 10093-10106, 10.5194/acp-15-10093-2015, 2015.

He, Q., Zhang, M., and Huang, B.: Spatio-temporal variation and impact factors analysis of satellite-based aerosol optical depth over China from 2002 to 2015, Atmos. Environ., Vol.129, 79-90, 10.1016/j.atmosenv.2016.01.002, 2016.

He, Q., Cao, J., Saide, P. E., Ye, T., and Wang, W.: Unraveling the Influence of Satellite-Observed Land Surface Temperature on High-Resolution Mapping of Ground-Level Ozone Using Interpretable Machine Learning, Environ. Sci. Technol., Vol.58, 15938-15948, 10.1021/acs.est.4c02926, 2024.

He, Q., Ye, T., Wang, W., Luo, M., Song, Y., and Zhang, M.: Spatiotemporally continuous estimates of daily 1-km $PM_{2.5}$ concentrations and their long-term exposure in China from 2000 to 2020, J. Environ. Manage., Vol.342, 118145, 10.1016/j.jenvman.2023.118145, 2023.

Jaffe, D.: Relationship between Surface and Free Tropospheric Ozone in the Western U.S, Environ. Sci. Technol., Vol.45, 432-438, 10.1021/es1028102, 2011.

Ke, L., Daniel J, J., Hong, L., Yulu, Q., Lu, S., Shixian, Z., Kelvin H, B., Melissa P, S., Shaojie, S., Xiao, L., Qiang, Z., Bo, Z., Yuli, Z., Jinqiang, Z., Hyun Chul, L., and Su Keun, K.: Ozone pollution in the North China Plain spreading into the late-winter haze season, Proceedings of the National Academy of Sciences of the United States of America, Vol.118, e2015797118, 10.1073/pnas.2015797118, 2021.

Li, J. and Li, Y.: Ozone deterioration over North China plain caused by light absorption of black carbon and organic carbon, Atmos. Environ., Vol.313, 120048, 10.1016/j.atmosenv.2023.120048, 2023.

Li, K., Jacob, D. J., Liao, H., Shen, L., Zhang, Q., and Bates, K. H.: Anthropogenic drivers of 2013–2017 trends in summer surface ozone in China, Proceedings of the National Academy of Sciences of the United States of America, Vol.116, 422-427, 10.1073/pnas.1812168116, 2019.

Li, R., Cui, L., Fu, H., Li, J., Zhao, Y., and Chen, J.: Satellite-based estimation of full-coverage ozone (O_3) concentration and health effect assessment across Hainan Island, J. Cleaner Prod., Vol.244, 118773, 10.1016/j.jclepro.2019.118773, 2020.

Li, S., WANG, T., ZANIS, P., MELAS, D., and ZHUANG, B.: Impact of Tropospheric Ozone on Summer Climate in China, J. Meteorolog. Res., 32, 279-287, 10.1007/s13351-018-7094-x, 2018.

Li, T. and Cheng, X.: Estimating daily full-coverage surface ozone concentration using satellite observations and a spatiotemporally embedded deep learning approach, Int. J. Appl. Earth Obs. Geoinf., Vol.101, 102356, 10.1016/j.jag.2021.102356, 2021.

Li, Z., Li, Q., and Chen, T.: Record-breaking High-temperature Outlook for 2023: An Assessment Based on the China Global Merged Temperature (CMST) Dataset, Adv. Atmos. Sci., 41, 369-376, 2024a.

Li, Z., Wang, W., He, Q., Chen, X., Huang, J., and Zhang, M.: Estimating ground-level high-resolution ozone concentration across China using a stacked machine-learning method, Atmos. Pollut. Res., Vol.15, 102114, 10.1016/j.apr.2024.102114, 2024b.

Liu, R., Ma, Z., Liu, Y., Shao, Y., Zhao, W., and Bi, J.: Spatiotemporal distributions of surface ozone levels in China from 2005 to 2017: A machine learning approach, Environ. Int., Vol.142, 105823, 10.1016/j.envint.2020.105823, 2020.

Liu, X., Zhu, Y., Xue, L., Desai, A. R., and Wang, H.: Cluster-Enhanced Ensemble Learning for Mapping Global Monthly Surface Ozone From 2003 to 2019, Geophys. Res. Lett., Vol.49, 1-13, 10.1029/2022gl097947, 2022.

Ma, R., Ban, J., Wang, Q., Zhang, Y., Yang, Y., Li, S., Shi, W., Zhou, Z., Zang, J., and Li, T.: Full-coverage 1 km daily ambient $PM_{2.5}$ and O_3 concentrations of China in 2005–2017 based on a multi-variable random forest model, Earth Syst. Sci. Data, Vol.14, 943-954, 10.5194/essd-14-943-2022, 2022a.

Ma, Z., Dey, S., Christopher, S., Liu, R., Bi, J., Balyan, P., and Liu, Y.: A review of statistical methods used for developing large-scale and long-term $PM_{2.5}$ models from satellite data, Remote Sens. Environ., Vol.269, 112827, 10.1016/j.rse.2021.112827, 2022b.

Maji, K. J. and Namdeo, A.: Continuous increases of surface ozone and associated premature mortality growth in China during 2015–2019, Environ. Pollut., Vol.269, 116183, 10.1016/j.envpol.2020.116183, 2021.

Mao, J., Wang, L., Lu, C., Liu, J., Li, M., Tang, G., Ji, D., Zhang, N., and Wang, Y.: Meteorological mechanism for a large-scale persistent severe ozone pollution event over eastern China in 2017, J. Environ. Sci., 92, 187-199, 2020.

Mashat, A. W. S., Awad, A. M., Alamoudi, A. O., and Assiri, M. E.: Monthly and seasonal variability of dust events over northern Saudi Arabia, Int. J. Climatol., Vol.40, 1607-1629, 10.1002/joc.6290, 2020.

Monks, P. S., Archibald, A. T., Colette, A., Cooper, O., Coyle, M., Derwent, R., Fowler, D., Granier, C., Law, K. S., and Mills, G. E.: Tropospheric ozone and its precursors from the urban to the global scale from air quality to short-lived climate forcer, Atmos. Chem. Phys., Vol.15, 8889-8973, 10.5194/acp-15-8889-2015, 2015.

Mu, X., Wang, S., Jiang, P., and Wu, Y.: Estimation of surface ozone concentration over Jiangsu province using a high-performance deep learning model, J. Environ. Sci., 132, 122-133, 2023a.

Mu, X., Wang, S., Jiang, P., Wang, B., Wu, Y., and Zhu, L.: Full-coverage spatiotemporal estimation of surface ozone over China based on a high-efficiency deep learning model, Int. J. Appl. Earth Obs. Geoinf., Vol.118, 103284, 10.1016/j.jag.2023.103284, 2023b.

Mukherjee, A., Agrawal, S. B., and Agrawal, M.: Intra-urban variability of ozone in a tropical city—characterization of local and regional sources and major influencing factors(Article), Air Qual. Atmos. Health, Vol.11, 965-977, 10.1007/s11869-018-0600-6, 2018.

Nicholas, N., Keith, S., Neal, F., Christopher G, N., Patrick, D., Tanya L, S., Perry, S., and Gregory A, W.: Ozone-related asthma emergency department visits in the US in a warming climate, Environ. Res., Vol.183, 109206, 10.1016/j.envres.2020.109206, 2020.

Qiao, X., Guo, H., Wang, P., Tang, Y., Ying, Q., Zhao, X., Deng, W., and Zhang, H.: Fine particulate matter and ozone pollution in the 18 cities of the sichuan basin in southwestern china: Model performance and characteristics(Article), Aerosol Air Qual. Res., Vol.19, 2308-2319, 10.4209/aaqr.2019.05.0235, 2019.

Ramya, A., Dhevagi, P., Poornima, R., Avudainayagam, S., Watanabe, M., and Agathokleous, E.: Effect of ozone stress on crop productivity: A threat to food security, Environ. Res., Vol.236, 116816, 10.1016/j.envres.2023.116816, 2023.

Rose, A., McKee, J., Sims, K., Bright, E., Reith, A., and Urban, M.: LandScan Global 2019 (2019), Oak Ridge National Laboratory [dataset], https://doi.org/10.48690/1524214, 2020.

Shang, N., Gui, K., Li, F., Li, B., Zhang, X., Zeng, Z., Zheng, Y., Li, L., Fei, Y., Peng, Y., Zhao, H., Yao, W., Liu, Y., Wang, H., Wang, Z., Wang, Y., Che, H., and Zhang, X.: Toward an Operational Machine-Learning-Based Model for Deriving the Real-Time Gapless Diurnal Cycle of Ozone Pollution in China with CLDAS Data, Environ. Sci. Technol. Lett., 11, 553-559, 10.1021/acs.estlett.4c00106, 2024.

Sharma, S., Sharma, P., and Khare, M.: Photo-chemical transport modelling of tropospheric ozone: A review, Atmos. Environ., Vol.159, 34-54, 10.1016/j.atmosenv.2017.03.047, 2017.

Shi, H., Song, X., and Zeng, S.: Impact of the Urban Heat Island Effect on Ozone Pollution in Chengdu City,China, Chin. Geogr. Sci., Vol.33, 1017-1032, 2023.

Sun, L., Xue, L., Wang, Y., Li, L., Lin, J., Ni, R., Yan, Y., Chen, L., Li, J., and Zhang, Q.: Impacts of meteorology and emissions on summertime surface ozone increases over central eastern China between 2003 and 2015, Atmospheric Chemistry & Physics, Vol.19, 1455-1469, 10.5194/acp-19-1455-2019, 2019.

Tu, J., Xia, Z., Wang, H., and Li, W.: Temporal variations in surface ozone and its precursors and meteorological effects at an urban site in China, Atmos. Res., Vol.85, 310-337, 10.1016/j.atmosres.2007.02.003, 2007.

Wang, N., Lyu, X., Deng, X., Huang, X., Jiang, F., and Ding, A.: Aggravating O_3 pollution due to NOx emission control in eastern China, Sci. Total Environ., Vol.677, 732-744, 10.1016/j.scitotenv.2019.04.388, 2019.

Wang, P., Yang, Y., Li, H., Chen, L., Dang, R., Xue, D., Li, B., Tang, J., Leung, L. R., and Liao, H.: North China Plain as a hot spot of ozone pollution exacerbated by extreme high temperatures, Atmos. Chem. Phys., Vol.22, 4705-4719, 10.5194/acp-22-4705-2022, 2022a.

Wang, T., Xue, L., Feng, Z., Dai, J., Zhang, Y., and Tan, Y.: Ground-level ozone pollution in China: a synthesis of recent findings on influencing factors and impacts, Environ. Res. Lett., 17, 063003, 10.1088/1748-9326/ac69fe, 2022b.

Wei, J., Li, Z., Li, K., Dickerson, R. R., Pinker, R. T., Wang, J., Liu, X., Sun, L., Xue, W., and Cribb, M.: Full-coverage mapping and spatiotemporal variations of ground-level ozone (O_3) pollution from 2013 to 2020 across China, Remote Sens. Environ., 270, 112775, https://doi.org/10.1016/j.rse.2021.112775, 2022.

Xia, Y., Hu, Y., Huang, Y., Bian, J., Zhao, C., Wei, J., Yan, Y., Xie, F., and Lin, J.: Concurrent hot extremes and high ultraviolet radiation in summer over the Yangtze Plain and their possible impact on surface ozone, Environ. Res. Lett., Vol.17, 064001, 10.1088/1748-9326/ac6c3c, 2022.

Xu, K., Lu, R., Mao, J., and Chen, R.: Circulation anomalies in the mid–high latitudes responsible for the extremely hot summer of 2018 over northeast Asia, Atmos. Oceanic Sci. Lett., Vol.12, 231-237, 10.1080/16742834.2019.1617626, 2019.

Xue, T., Zheng, Y., Geng, G., Xiao, Q., Meng, X., Wang, M., Li, X., Wu, N., Zhang, Q., and Zhu, T.: Estimating Spatiotemporal Variation in Ambient Ozone Exposure during 2013-2017 Using a Data-Fusion Model, Environ. Sci. Technol., Vol.54, 14877-14888, 10.1021/acs.est.0c03098, 2020.

Yang, Y., Zhou, Y., Wang, H., Li, M., Li, H., Wang, P., Yue, X., Li, K., Zhu, J., and Liao, H.: Meteorological characteristics of extreme ozone pollution events in China and their future predictions, Atmos. Chem. Phys., Vol.24, 1177-1191, 10.5194/acp-24-1177-2024, 2024.

Zhan, Y., Luo, Y., Deng, X., Grieneisen, M., Zhang, M., and Di, B.: Spatiotemporal prediction of daily ambient ozone levels across China using random forest for human exposure assessment, Environ. Pollut., Vol.233, 464-473, 10.1016/j.envpol.2017.10.029, 2018.

Zhang, X. Y., Zhao, L. M., Cheng, M. M., and Chen, D. M.: Estimating Ground-Level Ozone Concentrations in Eastern China Using Satellite-Based Precursors, IEEE Trans. Geosci. Remote Sens., Vol.58, 4754-4763, 10.1109/tgrs.2020.2966780, 2020.

Zhu, Q., Bi, J., Liu, X., Li, S., Wang, W., Zhao, Y., and Liu, Y.: Satellite-Based Long-Term Spatiotemporal Patterns of Surface Ozone Concentrations in China: 2005-2019, Environ. Health Perspect., Vol.130, 27004, 10.1289/ehp9406, 2022.